NMR Studies of Defensin Antimicrobial Peptides. 2. Three-Dimensional Structures of Rabbit NP-2 and Human HNP-1†

Arthur Pardi,*,‡ Xiao-Lu Zhang,§,‖ Michael E. Selsted,⊥ Jack J. Skalicky,‡ and Ping F. Yip‡,#

Department of Chemistry and Biochemistry, University of Colorado at Boulder, Boulder, Colorado 80309-0215, Department of Pathology, University of California College of Medicine, Irvine, California 92717, and Department of Chemistry, Rutgers, The State University of New Jersey, New Brunswick, New Jersey 08903

Received May 21, 1992; Revised Manuscript Received August 22, 1992

ABSTRACT: The solution structure of two homologous naturally occurring antimicrobial peptides, rabbit defensin NP-2 and human defensin HNP-1, have been determined by two-dimensional nuclear magnetic resonance spectroscopy, distance geometry, and restrained molecular dynamics calculations. The structure of these defensins consists of an antiparallel β-sheet in a hairpin conformation, a short region of triple-stranded β-sheet, several tight turns, and a loop region that has a well-defined local structure but with a global orientation that is not well-defined with respect to the rest of the molecule. The solution structures of these two peptides are compared with the solution and crystal structures of two other homologous defensins. The structures for the defensins are also compared with known structures of other naturally occurring antimicrobial peptides.

In recent years, a variety of naturally occurring antimicrobial peptides have been described. These include peptides from insects and worms [e.g., cecropins; reviewed in Boman (1991) and Boman et al. (1991)], crustaceans [e.g., tachplesins (Miyata et al., 1989)], lower vertebrates [e.g., magainins (Bevins & Zasloff, 1990)], and mammals [e.g., defensins (Lehrer et al., 1991) and bactenecins (Gennarro et al., 1991)]. The anatomic distribution in the host organism varies among species and includes the hemolymph of insects (Boman, 1991), circulating and tissue leukocytes (Lehrer et al., 1991; Miyata et al., 1989), epithelium including skin (Bevins & Zasloff, 1990; Mor et al., 1991), tracheal mucosa (Diamond et al., 1991), and intestinal mucosa (Ouellette et al., 1992). Some of these peptides possess potent, broad spectrum antimicrobial activities against bacteria, fungi, and viruses in vitro and thus have been considered as potential therapeutic antiinfectives. Alternatively, from knowledge of the three-dimensional structures of these peptides, it may be possible to design more readily synthesized and easily administered nonpeptide pharmaceuticals that possess similar antimicrobial activities. Unfortunately, the three-dimensional structures for few antimicrobial peptides have been determined, and there are few data on structure–activity relationships available to assist in determining the molecular requirements for their antimicrobial activities. Biophysical and physiological studies indicate that defensins, magainins, and cecropins can permeabilize biological membranes, suggesting that these peptides inactivate the target organism by altering essential properties at this site on the target envelope.

Knowledge of the three-dimensional structures of antimicrobial peptides would clearly aid in understanding their molecular modes of action and their broad spectra of activities and potencies. The three-dimensional structures for two naturally occurring defensin peptides have been previously reported: the solution structure of rabbit NP-5[1] (Bach et al., 1987; Pardi et al., 1988; Levy et al., 1989) and the crystal structure of human HNP-3 (Hill et al., 1991). Here we present the NMR solution structures of two additional defensin peptides, rabbit NP-2 and human HNP-1. HNP-1 and HNP-3, which differ in sequence by only a single N-terminal amino acid residue, possess distinctly different in vitro antimicrobial activities (Ganz et al., 1985), indicating that the amino terminus is a mechanistically important locus in these defensins. The 16 defensins characterized to date possess a broad spectrum of activities and a wide range of potencies (Lehrer et al., 1985, 1991; Ganz et al., 1985; Lichtenstein et al., 1986; Segal et al., 1985; Selsted & Harwig, 1987; Ouellette et al., 1992). The four defensins for which there are now three-dimensional structures span the full range of potencies and activities of all the known defensin peptides; thus the defensins provide an excellent model system for probing structure–activity relationships on biologically active peptides. The solution structures of the defensin peptides will also be compared with structural information on other naturally occurring antimicrobial peptides.

MATERIALS AND METHODS

The methods used for sample preparation and for acquisition and processing of the NMR data are given in the preceding paper (Zhang et al., 1992).

† This work was supported in part by funds from NIH Grants AI 22931 and AI 31696 to M.E.S. and by the Searle Scholars Program of the Chicago Community Trust (85-C110) and NIH Grant AI 27026 to A.P. A.P. is the recipient of a NIH Research Career Development Award 1991–1996 (AI 01051). The 400-MHz NMR spectrometer was purchased with partial support from NSF Grant CHEM-8300444, and the 500-MHz NMR spectrometer was purchased with partial support from NIH Grant RR03283. The molecular dynamics calculations were performed on the Cray Y-MP at the National Center for Supercomputing Applications at the University of Illinois, Urbana-Champaign.

* Author to whom correspondence should be addressed.

‡ University of Colorado at Boulder.

§ Rutgers.

‖ Present address: Pharmaceuticals Division, Ciba-Geigy Corp., 556 Morris Ave., Summit, NJ 07901.

⊥ University of California College of Medicine, Irvine.

Present address: Biosym Technologies Inc, 10065A Barnes Canyon Rd., San Diego, CA 92121.

[1] Abbreviations: NP-5 rabbit neutrophil peptide 5; NP-2 rabbit neutrophil peptide 2; HNP-1, human neutrophil peptide 1; HNP-3, human neutrophil peptide 3; 2D, two dimensional; NOE, nuclear Overhauser effect; $d_{\alpha N}$, distance from the C^{α} proton on residue i to the NH of residue $i+1$ in a polypeptide; MD, molecular dynamics; rms, root mean squared.

0006-2960/92/0431-11357$03.00/0

Distance Geometry Calculations. The distance constraints used in the structure calculations were derived from measurement of cross peak volumes in the 100- and 150-ms 2D NOE data sets for NP-2 and HNP-1, respectively. For the 2D NOE spectra in ^2H_2O of both peptides, the cross peak between the C^α protons of Gly^{24} was used as a calibration for calculating other proton–proton distances with these C^α protons assumed to be separated by 1.8 Å. For the NP-2 2D NOE data in H_2O, the $d_{\alpha N}$ interaction (Wüthrich, 1986) between residues 26 and 27 gives the largest resolved cross peak in the spectrum and was used to calibrate the other NOE-derived distances in the spectrum (a $d_{\alpha N}$ distance of 2.2 Å was assumed for this residue); however, in HNP-1 the $d_{\alpha N}$ cross peak between Ala^{12} and Gly^{13} was used for this calibration. The effects of spin diffusion or local motions were ignored in calculating the distance constraints for these peptides. Thus only qualitative interresidue distance constraints were included in the calculations, and the distances were input with bounds of ±0.5 Å for sequential and ±1.0 Å for nonsequential NOEs in the distance geometry algorithm. No effort was made to define the stereochemistry of prochiral protons. Instead, for the distance geometry calculations, the chirality constraint was relaxed for prochiral protons that had resolved chemical shifts (Pardi et al., 1988); however, for prochiral protons with degenerate chemical shifts, correction terms were added to the upper bound (Wüthrich et al., 1983). Correction terms were also added to NOEs involving methyl groups, as previously described (Pardi et al., 1988). A total of 62 sequential and 42 nonsequential distance constraints were included in the distance geometry calculations of NP-2. In addition, three disulfide bonds (Cys^5–Cys^{20}, Cys^{10}–Cys^{30}, Cys^3–Cys^{31}) and four hydrogen bonds (Cys^{20} NH···O=C His^{27}, Ile^{22} NH···O=C Arg^{25}, Arg^{25} NH···O=C Ile^{22}, His^{27} NH···O=C Cys^{20}) were included in the distance constraints used to define the structure of the peptide. For HNP-1, a total of 64 sequential and 65 nonsequential distance constraints were used in the distance geometry calculations along with the same disulfide and backbone hydrogen-bonding distance constraints used in the NP-2 calculations [a complete list of the NOEs for NP-2 and HNP-1 is given in Zhang (1989)]. As discussed in the preceding paper, for HNP-1, proline 8 was found to have a cis peptide bond, and so the covalent constraints for this residue included a cis peptide bond. The distance geometry calculations were carried out on a μVAX II computer with the DSPACE program (Hare Research, Inc.).

Molecular Dynamics Refinement. The starting structures for the molecular dynamics calculations were the distance geometry structures of NP-2 and HNP-1 generated as described above and the previously reported distance geometry structures for NP-5 (Pardi et al., 1988). All the distance constraints used in the distance geometry calculations were included as input for molecular dynamics calculations except that the distance bounds were modified with the constraints classified into three categories. For distances ≤2.8 Å, the bounds were ±0.5 Å; for distances between 2.8 and 3.7 Å, the bounds were −0.5 and +1.0 Å; and for distances ≥3.7 Å, the bounds were ±1.0 Å. In addition, 29 and 25 ϕ torsion angle constraints derived from the $^3J_{HN\alpha}$ coupling constraints were included in the refinement of the NP-2 and NP-5 structures, respectively. These ϕ torsion angles were calculated on the basis of a Karplus equation using the empirical parameters derived from model protein studies (Pardi et al., 1984). Multiple well potentials were used when the J coupling constant did not define a single range of torsion angles. The molecular dynamics refinements started from the distance geometry structures and employed the program AMBER 4.0. The dynamics simulations consisted of 2000 steps of conjugate gradient energy minimization followed by 6 ps of restrained molecular dynamics and finished with 2000 steps of restrained energy minimization. The restrained molecular dynamics procedure is similar to those previously reported (Gippert et al., 1990; Brünger & Karplus, 1991) and consisted of heating the system to 1000 K for 2 ps using a temperature relaxation time of 0.2 ps. The NMR distance and angle restraint weighting was gradually increased from 0.1 to 2.0 during this time [1.0 is the standard weighting and corresponds to force constants of 32 kcal/(mol·Å^2) for distance constraints and 32 kcal/(mol·rad^2) for angle constraints (Moore et al., 1988)]. This was followed by gradual cooling for 4 ps toward 0 K with a temperature relaxation time of 0.4 ps. During the cooling step, the NMR constraint weighting was decreased from 2.0 to 1.0. The force constants for all nonbonded terms (van der Waals, electrostatic, and hydrogen bonding) were the standard AMBER default values, but the weighting for these terms was set to 0.1 at the beginning of the refinement and was increased to a final value of 1.0 after 3 ps. The molecular dynamics and energy minimization calculations were carried out on a Cray Y-MP or a Silicon Graphics 4D/35TG computer.

RESULTS AND DISCUSSION

The strategy for determining the three-dimensional structures of the defensins was to use the distance geometry algorithm to generate starting structures that were then refined with molecular dynamics (MD) calculations and subsequently used in the structural comparisons.

Distance Geometry and Molecular Dynamics Calculations. The distance geometry algorithm is commonly used to generate starting structures for NMR solution structure determinations (Wüthrich, 1986); however, the algorithm has several potential weaknesses with one being production of local or global mirror image structures (Levy et al., 1989). Since chirality information is not included in the embedding process, right- and left-handed conformations of a structure can be obtained. However, given a sufficient number of NOE distance constraints, this is normally a minor problem since only one class of these structures can usually be refined to give low-energy conformations consistent with the NMR distance data. In this work, 10–20 independent runs of the distance geometry algorithm were performed for each peptide, and <30% of the structures were "mirror image" type structures where extensive simulated annealing type refinement did not lead to structures with small distance violations. Only those structures that had no distance violations >0.5 Å at the end of the distance geometry refinement were used in the subsequent molecular dynamics refinement, and all of these had the same global chirality.

A second problem that has been observed in earlier implementations of the metric-matrix distance geometry algorithm is inadequate sampling of conformational space (Havel & Wüthrich, 1985; Wagner et al., 1987; Metzler et al., 1989). Thus we previously used a Monte Carlo algorithm to generate three-dimensional structures of NP-5, in order to search for all structures consistent with the NMR distance information (Levy et al., 1989). These results showed that the three-dimensional fold observed in the distance geometry calculations was the only structure consistent with the NMR data. Thus, it appears that the defensin peptides contain enough long-range distance constraints, from the NOEs, J

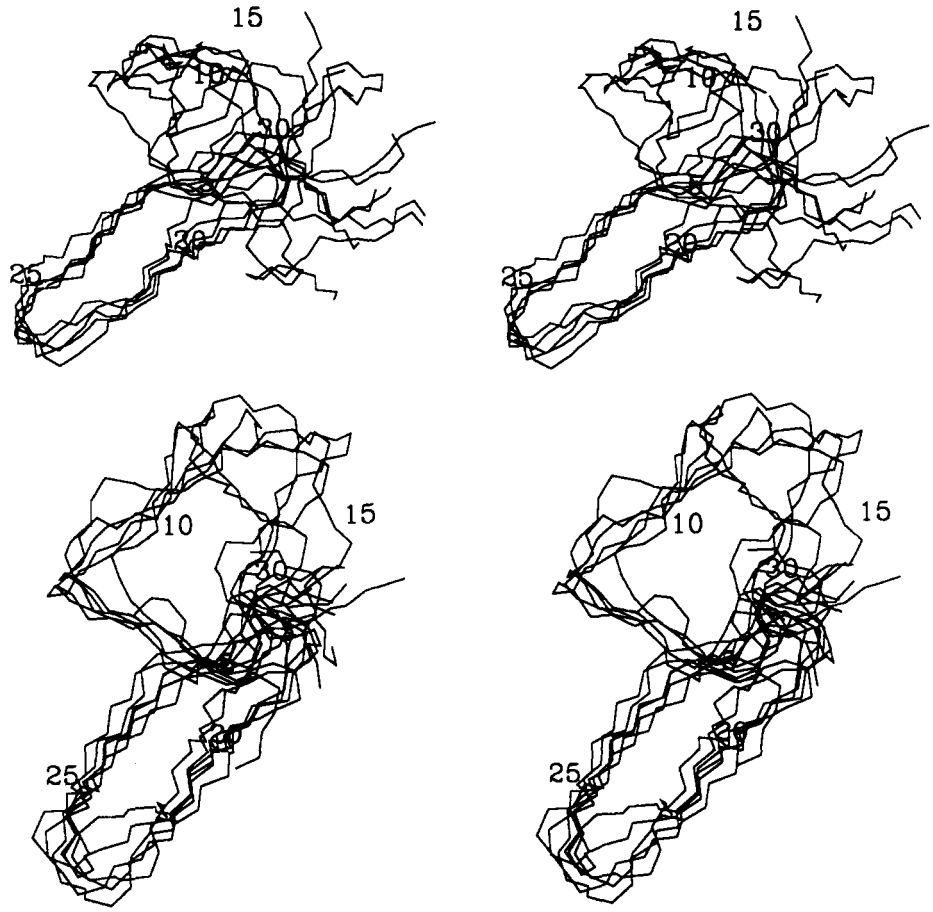

FIGURE 1: Stereopair of the superposition of (a, top) five NP-2 and (b, bottom) six HNP-1 structures derived from the restrained MD calculations. Only the C^{α}, C, and N atoms are shown, and the superpositions were best fits of these atoms for residues 15–30 in the β-sheets.

Table I: Distance and Angle Violations and Pairwise rms Distance Deviations for Select Backbone Regions of Defensins NP-2, HNP-1, and NP-5

av. no. of torsion and distance constraint violations per individual structure	NP-2 (n = 5)	HNP-1 (n = 6)	NP-5 (n = 7)
torsion angles >10°	1.6	–[a]	1.4
torsion angles >5° and ≤10°	1.6	–	3.3
torsion angles >1° and ≤5°	8.8	–	12.0
distances >0.2 Å	3.2	0.0	2.0
distances >0.1 and ≤0.2 Å	4.6	1.9	4.3
distances >0.05 and ≤0.1 Å	6.0	5.9	6.1
av pairwise rms (Å) for select backbone regions			
residues 2–31	3.0 ± 1.0	2.3 ± 0.5	2.4 ● 0.4
residues 3–7, 16–30	2.2 ± 0.7	1.5 ± 0.3	1.9 ± 0.9
residues 19–29	1.3 ● 0.3	1.3 ± 0.3	1.3 ● 0.4
residues 6–14	1.2 ± 0.2	1.9 ± 0.4	1.9 ± 0.6

[a] Not included in the calculations.

coupling constants and disulfide bonds, to determine the correct folding of the defensins.

In order to more adequately sample local structural variations consistent with the NMR data, the distance geometry structures were refined with molecular dynamics calculations as described under Materials and Methods.

Refined NP-2 Structures. Figure 1a shows a superposition of the peptide backbone for five NP-2 structures. In an NMR structure determination, different regions of structure may be better defined than others, and this is clearly the case in defensins. Thus we have chosen to superimpose the β-sheet region that has a low rms distance deviation in these structures. Another important parameter in judging the quality of NMR structures is the extent to which the final structures violate the input distance and torsion angle constraints. Table I gives the pairwise average rms distance deviations for various regions of NP-2 as well as the average number of distance and torsion angle violations in the final structures. These rms distance deviations indicate that the local structure is reasonably well-defined, but there is conformational variability for certain regions of the global structure. For example, as seen in Table I the average rms distance deviation of the peptide backbone for regions 2–31, 3–7 and 16–30, and 19–29 is 3.0, 2.2, and 1.3 Å, respectively. These data indicate that the β-hairpin region (residues 19–29) of NP-2 is better defined from the NMR data than other regions. Figure 1a also shows that the global geometry of residues 6–14 is not well-defined with respect to the rest of the peptide. This is not surprising since there are no nonsequential NOE connecting residues 6–14 to other parts of the peptides (see Figure 4a in the preceding paper in this issue). These results are similar to what was previously observed for the NMR solution structures of NP-5 (Pardi et al., 1988).

As seen in Figure 2a, the β-hairpin in NP-2 extends from approximately residue 15 to 31 and possesses the distinctive right-handed twist found in antiparallel β-sheets. As discussed in the preceding paper (Zhang et al., 1992), this β-hairpin also contains a β-bulge at residues Gly^{18}. In addition to the β-hairpin, there is a short piece of three-stranded β-sheet consisting of one end of the β-hairpin and the N-terminal residues in the peptide. The Cys^{3}–Cys^{31} disulfide bond links residues on two strands of this short triple-stranded region and is probably instrumental in stabilizing its formation.

NP-2 also possesses two tight turns involving residues 22–25 and 11–14. There are significant variations in the ϕ,ψ

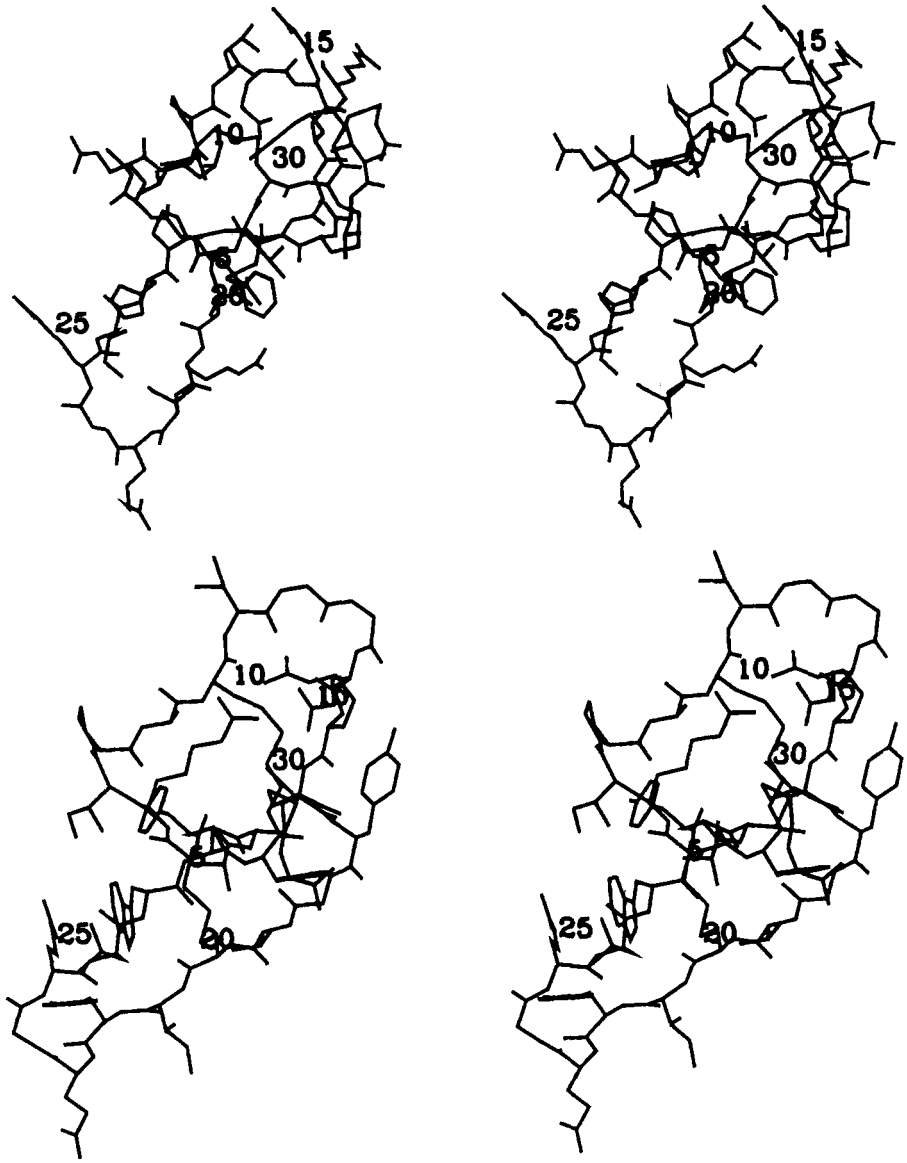

FIGURE 2: Stereopair of the lowest energy restrained MD structure of (a, top) NP-2 and (b, bottom) HNP-1. All heavy atoms are shown.

angles of these turns among the five NP-2 solution structures, and therefore neither turn could be classified into a unique turn type (Creighton, 1984).

Refined HNP-1 Structures. The number and location of the cysteine residues is readily determined from the primary structure of the peptide; however, the identification of disulfide linkages is generally more difficult to determine. To try to determine the disulfide linkages in HNP-1, two sets of distance geometry calculations were performed with different disulfide linkages. In both calculations, the Cys^5–Cys^{20} disulfide was included because this linkage was easily defined from qualitative analysis of the NOE data. These data also indicated that the only possible pairings for the other disulfides were (Cys^3–Cys^{31}, Cys^{10}–Cys^{30} or Cys^3–Cys^{30}, Cys^{10}–Cys^{31}). Independent distance geometry structure calculations were performed for these two pairings. The large residual distance violations for the Cys^3–Cys^{30}, Cys^{10}–Cys^{31} structures (data not shown) indicated that the only set of disulfide linkages consistent with the NMR distance constraints is Cys^5–Cys^{20}, Cys^3–Cys^{31}, and Cys^{10}–Cys^{30}. This set of disulfide linkages was independently identified by biochemical analysis (Selsted & Harwig, 1989).

Figure 1b shows a superposition of the peptide backbone for six NMR structures of HNP-1. The NMR solution structure for HNP-1 is quite similar to the NP-2 and NP-5 solution structures (Pardi et al., 1988). The average rms distance deviations for the pairwise superposition of various regions of HNP-1 are given in Table I and are again similar to those for NP-2 and NP-5. As seen in Figure 2b, HNP-1 possesses a β-hairpin (residues 15–30), a short region of triple-stranded β-sheet, and a β-bulge (at Gly^{18}). In addition, residues 22–25 and 11–14 form β-turns in HNP-1, but, as observed for NP-2, these turns could not be uniquely classified as to turn type due to variations in their ϕ,ψ angles.

Intermolecular Aggregation of HNP-1. HNP-1 has significantly more slowly exchanging amide protons than NP-2 or NP-5 [see Table III in the preceding paper (Zhang et al., 1992) and Bach et al. (1987) and Pardi et al. (1988)]. Some of these additional slowly exchanging amide protons in HNP-1 are on the surface of the molecule (see Figure 2b) and would be predicted to have fast hydrogen exchange rates (Wagner & Wüthrich, 1982; Wüthrich, 1986). The large number of slowly exchanging amide protons indicates that HNP-1 is not a monomer in solution and that the lifetime of the free monomer is much less than the lifetime for hydrogen exchange of a solvent-accessible amide proton [which is >100 s at pH 3.5 (Wüthrich, 1986)]. HNP-1 also shows larger proton resonance line widths and larger NOEs as compared to NP-2 or

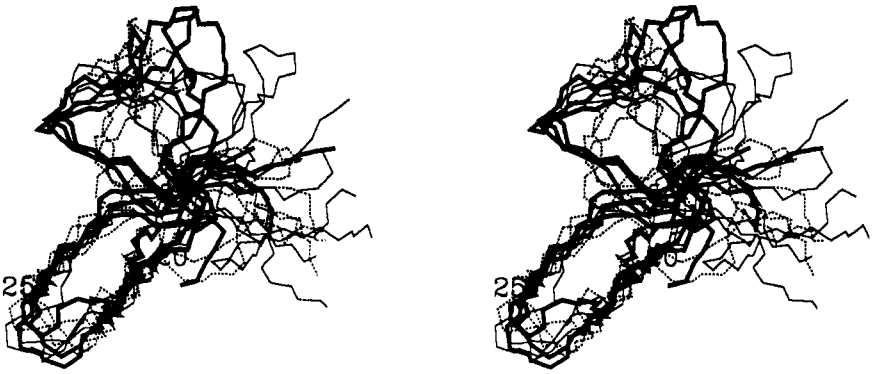

FIGURE 3: Stereopair showing the comparison of the backbone conformations for three restrained MD structures for HNP-1 (shown with bold solid lines), NP-2 (shown with thin solid lines), and NP-5 (shown with dashed lines). The superposition of the structures was performed using the backbone atoms in residues 15–30 of the β-sheets.

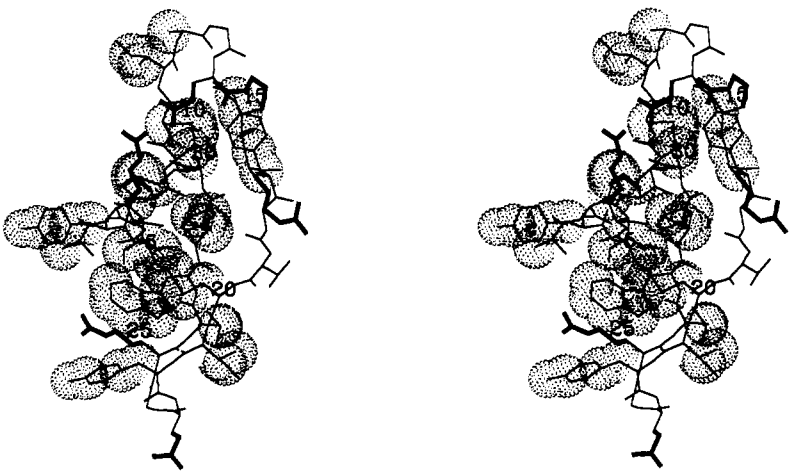

FIGURE 4: Stereopair of the lowest energy restrained MD structure of HNP-1 where the polar side chains are shown in bold and the side chains of the hydrophobic amino acids are shown with their van der Waals surfaces. The amino acid residues were classified according to the criteria of Rose et al. (1985) except that the tyrosine residues were classified as hydrophobic in the figure.

NP-5 (Bach et al., 1987), indicating that HNP-1 does not exist as a monomer under the NMR conditions used.

The stoichiometry of the HNP-1 complex could not be determined from the NMR data. However, our results are consistent with one or both of the following models: (i) HNP-1 forms a symmetrical complex in solution, or (ii) the rate of exchange between monomer and aggregate is fast on the NMR chemical shift time scale (milliseconds). If HNP-1 exists as a stable, slowly exchanging, asymmetric dimer in solution, distinct NMR resonances would be observed for some or all of the protons in each asymmetric unit. Since only a single resonance is observed for all protons in HNP-1, any stable slowly exchanging aggregate must have a center of symmetry where all the individual monomers are equivalent. However, this is not the only explanation for the data. The molecule could also exist as an asymmetric aggregate where the exchange between monomer and aggregate is fast on the NMR chemical shift time scale. Under these conditions, only a single resonance would be observed for each proton in the molecule. The present NMR data cannot distinguish between these possibilities.

Even though there is clear evidence of intermolecular aggregation of HNP-1 in solution, no intermolecular NOEs were observed in the molecule. Thus a dimer or higher order aggregate could not be built from direct NOE data. The location of slowly exchanging amide protons can help to define solvent-inaccessible surfaces in a molecule (Wagner & Wüthrich, 1982; Wüthrich, 1986), but we were unable to generate a model of a symmetrical dimer that has the slowly exchanging amide protons of both residues 21 and 26 solvent-inaccessible. As will be discussed below, the X-ray structure of HNP-3 is a symmetrical dimer where residue 21, but not residue 26, is solvent-inaccessible.

Comparison of the Solution Structures of the Defensins. Figure 3 shows the solution structures of the three defensins NP-2, NP-5, and HNP-1 where the backbone atoms in the β-hairpins of the three peptides have been superimposed. The three defensins have similar backbone folds. In the previous structure determination of NP-5 (Pardi et al., 1988), we did not identify the short third strand of β-sheet involving the N-terminal residues because, as seen in Figure 7 in the preceding paper (Zhang et al., 1992), NP-5 shows no cross-strand backbone NOEs for this antiparallel β-sheet whereas NP-2 and HNP-1 have two and three such NOEs, respectively. Thus the third strand of β-sheet is better formed for the latter two peptides than for NP-5. However, even with no cross-strand NOEs in NP-5, the peptide backbone of the N and C termini are held together by the Cys^3–Cys^{31} disulfide bond and have an antiparallel orientation (Pardi et al., 1988) that is qualitatively similar to the triple-stranded β-sheet observed in NP-2 and HNP-1.

The mechanism of action of the defensins is proposed to involve membrane permeabilization, and since these peptides contain a large number of hydrophobic and charged residues, the amphiphilicity of the solution structures of the defensins was analyzed. Figure 4 shows the structure of HNP-1 where the charged side chains are highlighted in bold and the hydrophobic side chains are highlighted by their van der Waals surfaces. Although the conformations of many of the side chains are not well determined from the present NMR data,

Table II: Average Pairwise rms Distance Deviation (Å) between the HNP-3 Crystal Structure and the NMR Structures for Defensins NP-2, HNP-1, and NP-5

selected backbone regions	HNP-3/ NP-2	HNP-3/ HNP-1	HNP-3/ NP-5
residues 2–30	4.5 ± 0.5	2.7 ± 0.4	3.4 ± 0.4
residues 3–7, 15–30	2.6 ± 0.6	1.8 ± 0.3	2.7 ± 0.3
residues 15–30	1.7 ± 0.4	1.6 ± 0.3	1.8 ± 0.4
residues 6–14	2.4 ± 0.1	1.7 ± 0.5	2.1 ± 0.3

the figure does show a distinctive hydrophobic surface for HNP-1. The charged residues generally face away from this surface, indicating that the peptide possesses an amphiphilic character. A salt bridge between Arg^6 and Glu^{14} is formed in the HNP-1 structure shown in Figure 4, and this salt bridge is on the hydrophobic surface of the molecule. However, it may be misleading to analyze the amphiphilic character of the defensin monomers since Hill et al. (1991) propose from their crystal structure of HNP-3 that the active structure for the peptide is a symmetrical dimer. Therefore the amphiphilic character of the dimer, and not the monomer, is likely the relevant factor in the mechanism of action of the peptide.

As seen in Figure 3, the most striking difference in the conformation of the three defensins is the relative orientation of the β-hairpin and the loop involving residues 6–14. NP-2 is the peptide with the widest variation in its global conformation and rms distance deviations (also see Table I). HNP-1 and NP-5 have similar, somewhat smaller, variations in their global structures (and rms distance deviations). Unfortunately, it is not possible to directly determine from our NMR data if the observed variations are due to flexibility of the peptides, and therefore could be related to their biological activities, or whether the variations are a result of limited NMR distance data for these regions of the peptides.

Comparison of the Solution and Crystal Structures of the Defensins. Hill et al. (1991) have generated a high-resolution crystal structure of HNP-3, and the overall folding is similar to that observed for the solution structures of NP-2, NP-5, and HNP-1. The solution structures of all three peptides were generated totally independently and reported prior to (Pardi et al., 1988; Zhang, 1989) the X-ray structure of HNP-3 (Hill et al., 1991). In fact, Eisenberg and co-workers initially attempted to solve the HNP-3 crystal structure by molecular replacement starting from the NMR solution structures of HNP-1, but this proved unsuccessful (Eisenberg and Hill, personal communication) possibly because the global conformation of the loop from residues 6–14 is not well-defined in the NMR structures. Thus the X-ray structure was subsequently solved by standard multiple isomorphous replacement techniques (Hill et al., 1991). The average pairwise rms distance deviations for all backbone atoms of the HNP-3 crystal structure and the HNP-1 solution structures is 2.7 Å (see Table II). However, as discussed above, the relative orientation of the β-hairpin and residues 6–14 is not well-defined in the NMR solution structures of HNP-1. Therefore, it is more appropriate to compare regions of the HNP-1 solution structure and the HNP-3 crystal structure, as opposed to the whole structure. Figure 5a shows a superposition of the backbone atoms for residues 15–30 of the HNP-3 crystal structure with the five HNP-1 solution structures. The X-ray structure shows a good fit with the solution structures with an average pairwise rms distance deviation of 1.8 Å (see Table II).

Figure 5b shows that the local structure for residues 6–14 is quite well-defined in the HNP-1 solution structures and has a backbone conformation similar to the HNP-3 crystal structure. The average rms distance deviation of the HNP-1 NMR structures from the HNP-3 crystal structure for this region is 1.7 Å (see Table II). There are several possibilities for why the global conformation of residues 6–14 is not well-defined relative to the rest of the peptide in the NMR solution structures. One may be that this region is dynamic and does not have a single rigid conformation in solution. A second is that there are no long-range NOEs from residues in this region to other parts of the molecule. Analysis of the HNP-3 crystal structure indicates that an important interaction that may help to determine the global conformation of residues 6–14 is the salt bridge between Arg^6 and Glu^{14}. No NOEs were observed between these residues in the NMR studies of HNP-1 (or NP-2 or NP-5), and therefore there is no direct NOE evidence to support formation of this salt bridge in solution. However, this salt bridge still forms in two of the six HNP-1 NMR structures, and one of these is the lowest energy structure shown in Figure 4. For these structures, it would appear to be the combination of the general proximity of these two residues and electrostatic attraction from the AMBER potential that drives formation of the salt bridge.

HNP-3 forms a symmetrical dimer in the X-ray structure, with the dimer being stabilized by an antiparallel β-sheet involving residues 17–22. As discussed above, the NMR experiments show clear evidence of a dimer or a higher order complex for HNP-1 in solution. However, no intermolecular NOEs were observed for HNP-1 in solution. The amide protons of residues 19 and 21 form cross-strand hydrogen bonds on the dimer interface in the HNP-3 crystal structure (Hill et al., 1991), and the amide proton of residue 21 is slowly exchanging in the solution studies of HNP-1, which is consistent with formation of the symmetrical dimer observed in HNP-3. However, the amide proton of residue 26 is also slowly exchanging in the NMR studies, and this result is not consistent with the HNP-3 crystal structure. The amide proton of residue 26 is fully solvent-accessible and not within hydrogen-bonding distance of any hydrogen-bond acceptors in the HNP-3 crystal structure. This anomalously slowly exchanging amide could result from the HNP-1 dimer forming a higher order, possibly nonspecific aggregate, in solution. Another possibility is that the molecule forms a number of intermolecular complexes (dimers or higher order aggregates) in solution that are all in fast exchange on the NMR time scale. In this case, the slow exchange of the amide proton of residue 26 would arise from formation of a complex where this proton is, on the average, inaccessible to solvent.

Structural Comparison of the Defensins with Other Naturally Occurring Antimicrobial Peptides. A wide variety of naturally occurring antimicrobial peptides have recently been identified with some of these functioning through oxygen-independent mechanisms primarily by disruption of membranes (Boman, 1991; Lehrer et al., 1991). Three-dimensional structures have been determined for only a few of these peptides, and these data show that a variety of structural motifs are employed in the mechanisms of action of antimicrobial peptides. We will briefly discuss peptides for which direct three-dimensional structural information is available, and their structures will be compared with the structures of the defensins.

The magainins are a class of small (18 amino acids) non-cysteine-containing cationic peptides that form amphiphilic α-helices, and their mechanism of action is thought to involve interaction with membranes (Zasloff, 1987; Bevins & Zasloff, 1990). Solution NMR studies on magainin 2 showed extensive amphiphilic helical structure in aqueous solutions containing 8% trifluoroethanol (Marion et al., 1988). The magainins

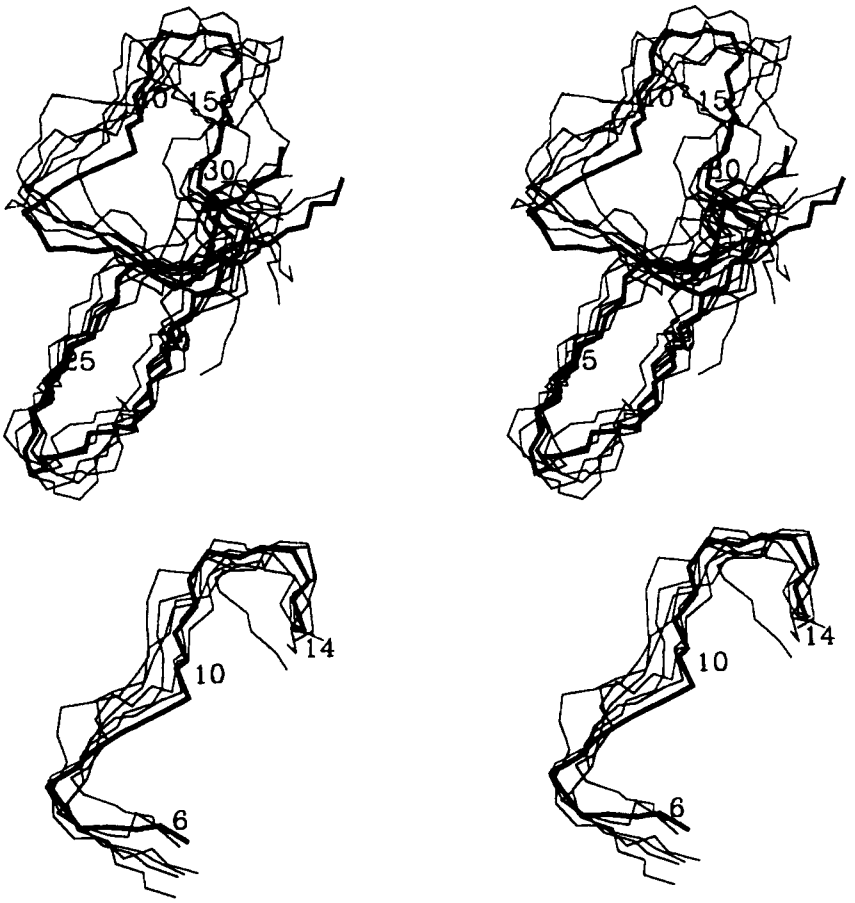

FIGURE 5: Stereopair of the NMR solution structures of HNP-1 and X-ray crystal of HNP-3 (a, top) where the backbone atoms for residues 16–30 were included in the superposition, and (b, bottom) where the backbone atoms for the loop involving residues 6–14 were included in the superposition. The X-ray structure is shown in bold, and six restrained molecule dynamics structures derived from the NMR data are shown with thin lines.

have been shown to lyse cells by formation of ion channels (Bevins & Zasloff, 1990), which is similar to the proposed mechanism of action of the defensins (Boman, 1991; Kagan et al., 1990; Lehrer et al., 1991). Most ion channel forming peptides are thought to form amphiphilic α-helical secondary structures (Lear et al., 1988).

The tachyplesins and polyphemusins represent another family of antimicrobial peptides (Miyata et al., 1989), and the solution structure of one tachyplesin has been determined (Kawano et al., 1990). These small (17–18 amino acid) highly basic peptides have been isolated from the hemocytes of horseshoe crabs. The peptides contain two disulfide linkages, and proton NMR studies of tachyplesin I indicate that it exists as an antiparallel β-sheet in a hairpin conformation in aqueous solution. Although a complete three-dimensional structure has not been reported, molecular modeling of this β-sheet reveals an amphiphilic structure where all the hydrophobic residues (including four aromatic residues, one valine, and one isoleucine) are on one face of the β-sheet with the charged residues generally clustered on the opposite face of the sheet (A. Pardi, unpublished results). The β-hairpin secondary structure and amphiphilic character of this peptide are structural features also found in the defensins. However, HNP-3 exists as a symmetrical dimer in the crystal, and Hill et al. (1991) propose that the active defensin species is a dimer or complex of dimers. These data suggest that the active species of tachyplesin I could be a higher order complex in solution.

The sapecins, or insect defensins, represent another class of antimicrobial peptides (Boman & Hultmark, 1987, Lee et al., 1989). These are small (40 amino acids) cationic peptides containing three disulfide linkages. The solution structure of the sapecin peptide has been determined (Hanzawa et al., 1990), and it has one loop region, a nine-residue α-helical region, and the C-terminal 16 amino acids form an antiparallel β-sheet in a hairpin conformation. The N-terminal amino acids are relatively well-defined in the solution structure and are in an orientation consistent with formation of a short region of triple-stranded β-sheet. The preliminary report of the structure of this peptide did not identify the presence of the short region of triple-stranded β-sheet (Hanzawa et al., 1990); however, Bontems et al. (1991) have determined the three-dimensional structure of charybdotoxin and propose that it has the same structural fold as sapecin. For charybdotoxin, the N-terminal residues clearly form a short region of triple-stranded antiparallel β-sheet, suggesting that the N-terminal residues in sapecin also form part of a triple-stranded β-sheet. The β-hairpin secondary structure, the short region of triple-stranded β-sheet, and the proposed amphiphilic nature of sapecin are structural features also observed in the defensins. However, it is not known if these two classes of peptides have similar mechanisms for their antimicrobial activities.

CONCLUSIONS

Solution structures have been determined for several homologous defensins that differ dramatically in their in vitro potencies and spectrum of antimicrobial activities. The human defensin HNP-1 and the rabbit defensin NP-2 show folding of the polypeptide backbone similar to the previously determined solution structure of rabbit NP-5 (Pardi et al., 1988)

and the crystal structure of human HNP-3 (Hill et al., 1991). The predominate solution structural features for the defensins are an antiparallel β-sheet in a hairpin conformation (residues ~15–30), a short region of triple-stranded β-sheet (involving this β-hairpin, and the N-terminal residues 2–5), several tight turns, and a loop region (residues 6–14) where the local structure of the loop is well-defined but the relative orientation of the loop with respect to the rest of the peptide is not well-defined in solution.

HNP-3 exists as a symmetrical dimer in the crystal structure whereas, although the solution NMR data on HNP-1 show clear evidence of a dimer or higher order aggregate in solution, it was not possible to define the structure of the dimer from NMR. The X-ray structure of the dimer explains almost all the hydrogen exchange data for the amide protons of HNP-1 with the only exception being the amide proton on residue 26. This proton is fully solvent-accessible in the X-ray crystal structure, and therefore would be predicted to have a fast exchange rate, but is found to be slowly exchanging in solution. We are presently unable to explain why this amide proton is slowly exchanging in solution; however, this result is consistent with HNP-1 forming a higher order complex than the dimer observed in the X-ray structure of HNP-3 (Hill et al., 1991).

The main difference between the solution and crystal structures is the variation for the peptide backbone of the loop involving residues 6–14. This region is globally disordered in the solution structure whereas it is well-ordered in the X-ray structure. From the present data, it is not possible to determine definitively whether this region is dynamic in solution or whether the disorder in the NMR structure is due to the absence of NOEs for this region of the peptide. The observation that the local structure of the loop is relatively well-defined whereas the loop is globally disordered (with respect to the rest of the molecule) in all three peptides, suggests that the loop region is dynamic in solution.

In summary, the solution structures of the defensins indicate a dynamic loop region that was not predicted from the X-ray structure, and the X-ray data revealed dimer formation that could not be identified from the NMR data. Thus the solution and crystal structure data on the defensins reveal structural and dynamic features that were not available from either technique alone and point out the usefulness of combining both NMR and X-ray structural data on biomolecules.

ACKNOWLEDGMENT

We thank Drs. C. P. Hill and D. Eisenberg for useful discussions.

REFERENCES

Bach, A. C., Selsted, M. E., & Pardi, A. (1987) *Biochemistry 26*, 4389–4397.

Bevins, C. L., & Zasloff, M. (1990) *Annu. Rev. Biochem. 59*, 395–414.

Boman, H. G. (1991) *Cell 65*, 205–207.

Boman, H. G., & Hultmark, D. (1987) *Annu. Rev. Microbiol. 41*, 103–126.

Boman, H. G., Faye, I., Gudmundsson, G. H., Lee, J. Y., & Lidholm, D. A. (1991) *Eur. J. Biochem. 202*, 849–854.

Bontems, F., Roumestand, C., Gilquin, B., Menez, A., & Toma, F. (1991) *Science 254*, 1521–1523.

Brünger, A. T., & Karplus, M. (1991) *Acc. Chem. Res. 24*, 54–61.

Creighton, T. E. (1984) *Proteins, Structures and Molecular Principles*, Freeman & Co., New York.

Diamond, G., Zasloff, M., Eck, H., Brasseur, M., Maloy, W. L., & Bevins, C. L. (1991) *Proc. Natl. Acad. Sci. U.S.A. 88*, 3952–3956.

Ganz, T., Selsted, M. E., Szklarek, D., Harwig, S. S., Daher, K., Bainton, D. F., & Lehrer, R. I. (1985) *J. Clin. Invest. 76*, 1427–1435.

Gippert, G. P., Yip, P. F., Wright, P. E., & Case, D. A. (1990) *Biochem. Pharmacol. 40*, 15–22.

Hanzawa, H., Shimada, I., Kuzuhara, T., Komano, H., Kohda, D., Inagaki, F., Natori, S., & Arata, Y. (1990) *FEBS Lett. 269*, 413–420.

Havel, T. F., & Wüthrich, K. (1985) *J. Mol. Biol. 182*, 281–294.

Hill, C. P., Yee, J., Selsted, M. E., & Eisenberg, D. (1991) *Science 251*, 1481–1485.

Kagan, B. L., Selsted, M. E., Ganz, T., & Lehrer, R. I. (1990) *Proc. Natl. Acad. Sci. U.S.A. 87*, 210–214.

Kawano, K., Yoneya, T., Miyata, T., Yoshikawa, K., Tokunaga, F., Terada, Y., & Iwanaga, S. (1990) *J. Biol. Chem. 265*, 15365–15367.

Lear, J. D., Wasserman, Z. R., & Degrado, W. F. (1988) *Science 240*, 1177–1181.

Lee, J. Y., Boman, A., Sun, C. X., Andersson, M., Jornvall, H., Mutt, V., & Boman, H. G. (1989) *Proc. Natl. Acad. Sci. U.S.A. 86*, 9159–9162.

Lehrer, R. I., Szklarek, D., Ganz, T., & Selsted, M. E. (1985) *Infect. Immun. 49*, 207–211.

Lehrer, R. I., Ganz, T., & Selsted, M. E. (1991) *Cell 64*, 229–230.

Levy, R. M., Bassolino, D. A., Kitchen, D. B., & Pardi, A. (1989) *Biochemistry 28*, 9361–9372.

Lichtenstein, A., Ganz, T., Selsted, M. E., & Lehrer, R. I. (1986) *Blood 68*, 1407–1410.

Marion, D., Zasloff, M., & Bax, A. (1988) *FEBS Lett. 227*, 21–26.

Metzler, W. J., Hare, D. R., & Pardi, A. (1989) *Biochemistry 28*, 7045–7052.

Miyata, T., Tokunaga, F., Yoneya, T., Yoshikawa, K., Iwanaga, S., Niwa, M., Takao, T., & Shimonishi, Y. (1989) *J. Biochem. (Tokyo) 106*, 663–668.

Moore, J. M., Case, D. A., Chazin, W. J., Gippert, G. P., Havel, T. F., Powls, R., & Wright, P. E. (1988) *Science 240*, 314–317.

Mor, A., Nguyen, V. H., Delfour, A., Migliore, S. D., & Nicolas, P. (1991) *Biochemistry 30*, 8824–8830.

Ouellette, A. J., Miller, S. I., Henschen, A. H., & Selsted, M. E. (1992) *FEBS Lett.* (in press).

Pardi, A., Billeter, M., & Wüthrich, K. (1984) *J. Mol. Biol. 180*, 741–751.

Pardi, A., Hare, D. R., Selsted, M. E., Morrison, R. D., Bassolino, D. A., & Bach, A. C., II (1988) *J. Mol. Biol. 201*, 625–636.

Rose, G. D., Geselowitz, A. R., Lesser, G. J., Lee, R. H., & Zehfus, M. H. (1985) *Science 229*, 834–838.

Segal, G. P., Lehrer, R. I., & Selsted, M. E. (1985) *J. Infect. Dis. 151*, 890–894.

Selsted, M. E., & Harwig, S. S. (1987) *Infect. Immun. 55*, 2281–2286.

Selsted, M. E., & Harwig, S. S. (1989) *J. Biol. Chem. 264*, 4003–4007.

Wagner, G., & Wüthrich, K. (1982) *J. Mol. Biol. 160*, 343–361.

Wagner, G., Braun, W., Havel, T. F., Schaumann, T., Go, N., & Wüthrich, K. (1987) *J. Mol. Biol. 196*, 611–639.

Wüthrich, K. (1986) *NMR of Proteins and Nucleic Acids*, John Wiley & Sons, New York.

Wüthrich, K., Billeter, M., & Braun, W. (1983) *J. Mol. Biol. 169*, 949–961.

Zasloff, M. (1987) *Proc. Natl. Acad. Sci. U.S.A. 84*, 5449–5453.

Zhang, X. L. (1989) Ph.D. Thesis, *Solution Structures of Antimicrobial Peptides Determined by Nuclear Magnetic Resonance Spectroscopy and Distance Geometry Techniques*, Rutgers University, New Brunswick, NJ.

Zhang, X. L., Selsted, M. E., & Pardi, A. (1992) *Biochemistry* (preceding paper in this issue).